Available online at www.sciencedirect.com

jmr&t Journal of Materials Research and Technology

journal homepage: www.elsevier.com/locate/jmrt

Original Article

Prediction of mechanical properties of AlTiCrVNb high entropy alloys with B2 ordered structure

Zuodong Zheng [a], Qingjun Chen [a,*], Xinyuan Peng [a], Hao Wang [b], Shoujiang Qu [c], Aihang Feng [c], Tong Xu [a], Kan Wang [a]

[a] School of Material Science and Engineering, Nanchang Hangkong University, Nanchang 330063, China
[b] Interdisciplinary Centre for Additive Manufacturing (ICAM), School of Materials and Chemistry, University of Shanghai for Science and Technology, Shanghai 200093, China
[c] School of Materials Science and Engineering, Tongji University, Shanghai 201804, China

ARTICLE INFO

Article history:
Received 28 December 2022
Accepted 5 March 2023
Available online 9 March 2023

Keywords:
B2 order
High entropy alloy
First-principles
Density functional theory
Mechanical properties

ABSTRACT

Chemical short-range order (CSRO) is widely reported and it's certainly related to high entropy alloys (HEAs)'s mechanical properties in many different correlative researches. B2 structure ordering is usually thought to improve alloy's structural stability and strength while sacrificing the plasticity significantly. In this work, we established a B2 ordered model by the special quasi-random structure method which considering the local atomic environment (to simulate the real situation in HEAs). Depending on this model and first principles, the elements' occupancy and the B2 structure ordering are considered to explore their influence on the mechanical properties of AlTiCrVNb HEAs. The B2-type partially ordered configuration was applied to non-iso atomic ratio alloys to investigate the different influence on alloys' mechanical properties due to the changing content of Ti or Cr and the results were verified by experiment.

1. Introduction

High entropy alloys (HEAs) is a new sort of multiple-primary elements alloys and always maintains a single solid solution phase. It was first reported by Yeh and Cantor et al., in 2004 [1,2] and it owns excellent mechanical properties and unique physical mechanism. As a potential engineering material using in high temperature situation, the existed refractory high entropy alloys (RHEAs) always composed of high-density elements [3–6]. In order to reduce density, Al is introduced into RHEAs wildly. A body-centered cubic (BCC) high-entropy alloy AlTiCrVNb with high specific strength is proposed with the premise of ensuring light weight and refractory. HEAs used to be thought as a typical disordered solid solution and the various atoms distributed in the lattice randomly, while recent studies spotted that the ordered structures may also formed in the HEAs due to the chemical complexity of multiple primary elements [7–11]. B2 ordered structure is a special BCC structure formed when the element occupies a specific lattice position. The B2 phase structure is usually found in BCC Aluminum-containing refractory alloys. A large part of B2 phase alloys exhibit some outstanding physical properties on

* Corresponding author.
E-mail address: qjchen@nchu.edu.cn (Q. Chen).
https://doi.org/10.1016/j.jmrt.2023.03.031

high temperature stability and oxidation resistant, while the lack of fracture toughness and ductility restricts its further application [9,12–15]. Thus, in order to design ductile AlTiCrVNb HEAs, it's essential to study how the B2 ordered effects on alloy's mechanical properties.

The main methods nowadays to study how the B2 phase effects the alloy's properties have always been based on experiment, while the simulation method is gaining popularity to analyze the distribution of elements in B2 phase and its effect on alloy properties [7,16,17]. Most of the current research B2 ordered simulation work is based on the coherence potential approximation (CPA) method. Although the properties of HEAs calculated by the CPA [18,19] method are consistent with the experimental results, the effective atoms are fictitious and the resulting environmental uniformity is uncertain. Besides, the CPA method cannot describe lattice distortions since it presumes that each atom is in a highly symmetric position and all lattice position are occupied identically-no force existed to move the atom from its own position. In contrast, the special quasi-random structure (SQS) method performs an outstanding simulating mechanism in presenting the real situation of atoms in the lattice, and the alloy atomic environment was considered as a factor affecting alloy's physicochemical properties. Therefore, to investigate the chemical ordering's effect on structural and mechanical properties of AlTiCrVNb HEAs, this work is based on the SQS method.

2. Calculation method

2.1. Build models

The iso atomic ratio AlTiCrVNb high-entropy alloy was modeled by the special quasi-random structure (SQS) method [20,21]of the Alloy Theoretic Automated Toolkit (ATAT) software, and disordered and ordered supercells were created separately for comparison, which contains 1 disordered supercell as well as 15 ordered supercells. As shown in Fig. 1a and b, the random BCC structure is expressed as α, the B2 ordered structure can be expressed as (α)-(β). In this work, the α and β sites are occupied by two elements respectively, and the remaining element is randomly distributed in α and β sites to balance the element concentration. For example $(AlCrV)_{\alpha}$-$(TiNbV)_{\beta}$ means that Al, Cr and V atoms occupy one of the sublattices α, and Ti, Nb and V atoms occupy the other

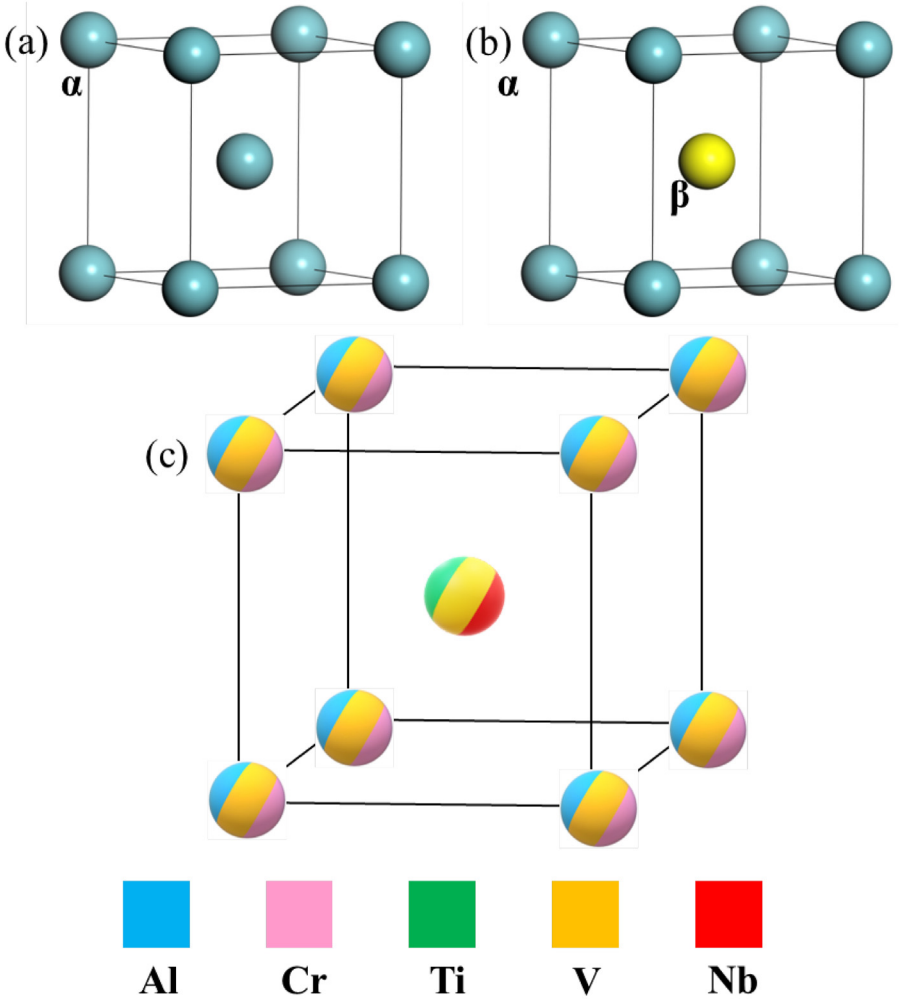

Fig. 1 – (a) Disordered BCC configuration. (b) Ordered B2 configuration. (c) Elements occupancy in B2 configuration.

sublattice β (inset of Fig. 1c), where V is the element used to balance the concentration, the other representations are the same.

The dimensions of all supercells for isomolar ratio alloys are 5 × 1 × 1, meaning that each supercell contains 10 atoms. The subsequent properties of $Ti_xCrVNbAl$ and $Cr_xTiVNbAl$ (where x = 0.5, 1, 1.5, 2) high entropy alloys were calculated based on the B2 ordered structure. When x was 0.5, 1.5, and 2, the size of the model supercell was 3 × 3 × 1, 11 × 1 × 1, and 5 × 2 × 1, respectively.

In order to differentiate between the BCC and B2 structures, various primitive cells were utilized in the modeling process. The primitive cell vectors of a body-centered cubic structure can be represented as $\overrightarrow{a1} = \frac{a}{2}(-\vec{i}+\vec{j}+\vec{k})$, $\overrightarrow{a2} = \frac{a}{2}(\vec{i}-\vec{j}+\vec{k})$, $\overrightarrow{a3} = \frac{a}{2}(\vec{i}+\vec{j}-\vec{k})$. Its meaning is to extend the base vectors from a vertex to the three body centers. Assuming the lattice constant 'a' is equal to 1, these three vectors can be represented as (−0.5, 0.5, 0.5) (0.5, −0.5, 0.5) (0.5, 0.5, −0.5). The primitive cell of a body-centered cube has 1 lattice point, so the point (0,0,0) can represent all the points in the BCC structure. B2 structure primitive cell base vectors can be expressed as (1, 0, 0) (0, 1, 0) (0, 0, 1). The primitive cell of a B2 structure has 2 lattice points. The coordinates (0, 0, 0) and (0.5, 0.5, 0.5) can represent all points of B2 structure.

2.2. Calculation details

All first principles calculations were performed using the Vienna Ab initio Simulation Package (VASP) based on density functional theory (DFT) [22,23]. The Perdew–Burke–Ernzerhof (PBE) functional [24,25] in the generalized gradient approximation (GGA) [26] is used to describe the exchange-correlation action. The electron–ion interaction was processed by the projector augmented wave (PAW) method [27,28]. After some strict convergence tests, the energy cutoff is set to 500eV, and the Brillouin zone is sampled using the special k-grid generated by the Monkhorst Pack [29] scheme with a k-point spacing of 0.03 $Å^{-1}$. Before the static calculation, conjugate gradient method (CG) is used to optimize the structure. The convergence tolerance of the total energy is 10^{-6}eV, and the Hellmann Feynman forces tolerance is set to 10^{-2}eV/Å.

Lattice parameters and bulk modulus are obtained by fitting the Birch–Murnaghan equation of state [30,31]. Subsequent calculations are based on fixed lattice constants. The B-M equation of state is shown in Equation (1):

Where E, E_0 represent total energy and steady state energy respectively. V, V_0 correspond to volume and equilibrium volume, and B and B′ are bulk modulus and the first derivative of bulk modulus.

$$E(V) = E_0 + \frac{9V_0B}{16}\left\{\left[\left(\frac{V_0}{V}\right)^{\frac{2}{3}}-1\right]^3 B' + \left[\left(\frac{V_0}{V}\right)^{\frac{2}{3}}-1\right]^2\left[6-4\left(\frac{V_0}{V}\right)^{\frac{2}{3}}\right]\right\} \quad (1)$$

The stress–strain method [32]was used to calculate the elastic constant matrix C_{ij}, and the elastic properties of the cubic crystalline system were characterized by three elastic constants, C_{11}, C_{12} and C_{44}. The polycrystalline shear modulus G is calculated from the Hill mean value of the single elastic constant [33]:

$$G = \frac{G_V + G_R}{2} \quad (2)$$

$$G_V = \frac{C_{11} - C_{12} + 3C_{44}}{5} \quad (3)$$

$$G_R = \frac{5(C_{11} - C_{12})C_{44}}{4C_{44} + 3(C_{11} - C_{12})} \quad (4)$$

G_R and G_V correspond to the values of Reuss and Voigt, respectively. The value of Young's modulus (E) is:

$$E = \frac{9BG}{3B + G} \quad (5)$$

Poisson's ratio (υ) can be expressed as:

$$\upsilon = \frac{3B - 2G}{2(3B + G)} \quad (6)$$

3. Results and discussion

The two sublattices in completely disordered BCC and B2 ordered structure perform differently-the B2 phases are not equivalent. The ratio of the number of atoms at the α-site to the β-site in the B2 structure is 1:1, so the distribution of the five elements in the AlTiCrVNb alloy should follow this condition. For example, in the equimolar ratio B2 configuration $(AlCrV)_\alpha$-$(TiNbV)_\beta$, Al and Cr contents at α-site are 40% and V content is 20%, respectively; Ti and Nb contents at β-site are 40% and V content is 20%, respectively. Due to this, 15 kinds of structures with different atomic distribution to simulate B2 phase are established. In order to verify the effect of chemical short-range order, the lattice constants of the crystal were calculated. Fig. 2a shows the calculation results of the lattice constant. The results show that the lattice constants range from 3.11 to 3.12 Å, with less than 0.16% fluctuation in lattice constants relative to the disordered structure. It shows that the occupancy of local atoms and lattice distortion are affected obviously by the chemical short-range order while the lattice constant is little affected by it. This may explain the limited influence range of chemical short-range order due to its composition which only includes the first and second nearest neighbor atoms. The experimentally measured lattice constant of the AlTiCrVNb alloy is 3.12 Å, and the maximum error among 16 calculated structures does not exceed 0.32%, indicating that the calculated result is reliable. The lattice constant's discrepancy between the ordered/disordered structure is so tiny that the X-ray diffraction is unable to distinguished. The simulation result, similar to the experimental result, provided the proof that the B2 phase existed.

The optimization of structure sought in the ordered configuration follows the principle of its energy difference compared with the disordered configuration that the lowest structure's total energy expresses the highest stability.

The calculation results show that the (V–Al–Cr) (V–Ti–Nb) configuration owns the lowest energy hence its structure is the most stable among all ordered models. That is, in this ideal

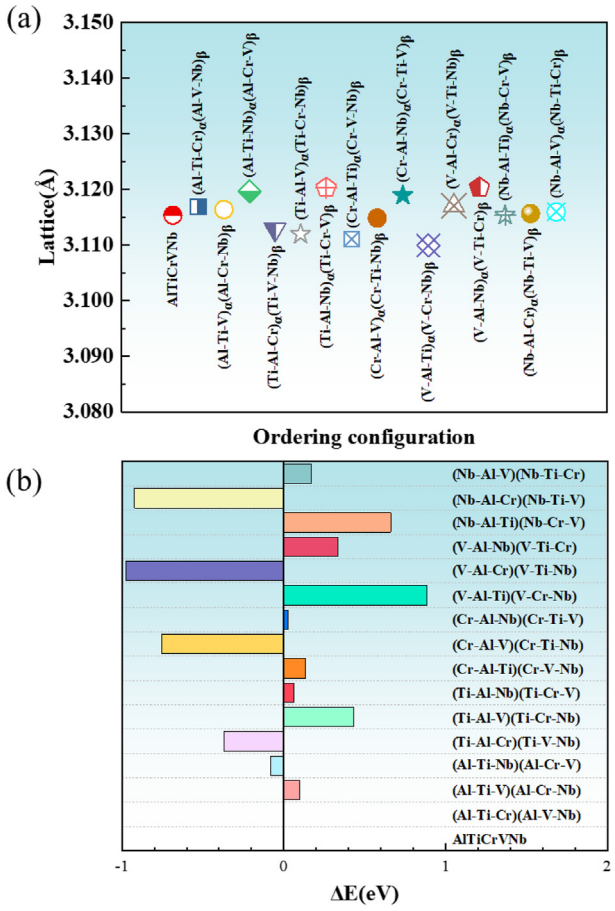

Fig. 2 – (a) Lattice constants for 16 different structures (b) Energy difference between ordered configuration and disordered configuration.

B2 configuration, Cr tends to occupy the sublattice of Al and Nb tends to occupy the sublattice of Ti, where V is randomly distributed in both sublattices to balance the concentration (V–Al–Cr) (V–Ti–Nb) configuration and disordered AlTiCrVNb configuration are used in the subsequent calculation to investigate how the chemical short-range order acts on alloy's mechanical properties.

A deeper understanding of phase stability can be obtained by analyzing the density of states (DOS) [34]. Fig. 3 shows the total density of states (TDOS) and partial of total density (PDOS) for ordered and disordered configurations. The dashed-line (at 0 eV) displays Fermi level (E_F) in Fig. 3. It can be seen obviously that TDOS of the two configurations at E_F enters the conduction band, indicating that both configurations exhibit metallic character. It's also worth mentioning that for two the configurations, the electronic band structure is dominated by d-states of Ti, V, Cr, Nb atoms with small admixture of s- and p-states of Al atoms. Moreover, Cr-d state has slightly stronger contributions than other elements. In addition, the PDOS shows d-states electrons are hybridized near the Fermi level. Due to this strong orbital hybridization, the alloys can exist stably. In order to clearly represent the DOS characteristics near the Fermi level, the DOS of the two configurations are enlarged and listed in Fig. 3c. Theoretical studies show that the value of DOS at E_F is closely related to the phase structural stability and mechanical properties: a low DOS value indicates that the alloy possesses a high phase stability [35,36]. The TDOS value of B2 configuration is about 8.3 electrons/eV, while disorder configuration is about 13.1 electrons/eV. It means that B2 configuration is more than disorder configuration and owns higher elastic modulus. However, more stable structure owns greater resistance to shear deformation that make the ductility worse.

In order to explore the effect of ordered structure of B2 on mechanical properties, the mechanical properties of disordered and ordered configurations were calculated first. According to the calculated values in Table 1, the order of B2 has a great influence on the mechanical properties of the alloy, for which the elastic constants C_{11} and C_{12} are more sensitive to whether the structure is ordered or not. Generally, the bulk modulus B indicates the resistance of volume changes when uniform pressure is applied, and the two configurations have little effect on the B of the alloy. The main difference is reflected in shear modulus G and Young's modulus E, the disordered configuration has less ability to resist shear strain and tensile deformation than the ordered B2 configuration. However, Poisson's ratio υ and Pugh's ratio of ordered B2 configuration are significantly smaller than those of disordered B2 configuration, indicating that B2 configuration improved the strength of the material while sacrificing the ductility. According to the experimental data, the strength and ductility of the alloy are similar to B2 configuration calculating value. The subsequent calculations in this study were based on the partially ordered B2 configuration.

The ordered model of $Ti_xCrVNbAl$ and Cr_x-TiVNbAl($x = 0.5,1.5,2$) high entropy alloys B2 was established by SQS method. Due to the change in alloy composition , the elemental content of each site is being allocated according to the elemental occupancy of the optimal B2 configuration (shown in Table 2). The mechanical properties of the alloys were compared with the experimental values to determine whether the mechanical properties of the alloys were closely related to the B2 ordered. The calculating result of alloys' lattice constants and density which based on the first-principle method due to the different Ti or Cr contents is exhibited on Fig. 4a and b. Compared with other elements (Al,Cr,V,Nb), Ti owns the largest atomic radius and the lowest density except Al. With the increase of Ti content, the lattice constant of the alloy increases, leading to the decrease of density. The lattice constant of the alloy decreases and the density increases with the increase of Cr content since the density of Cr is the largest and the atomic radius is the smallest.

Elastic constants usually determine the elastic properties of materials and directly reflect the mechanical properties. Fig. 4c and d shows the calculated elastic constants of Ti_x-CrVNbAl and Cr_xTiVNbAl high-entropy alloys. The criterion of mechanical stability [37]: $C_{11} > 0$, $C_{44} > 0$, $C_{11}-C_{12} > 0$ and $C_{11}+2C_{12} > 0$, so all alloys are mechanically stable. The values of C_{ij} are variable due to the variation of Ti content, C_{11} gained the maximum 236.34 GPa when $x = 0.5$ and the minimum 195.04 GPa when $x = 2$, changing range is 41.3 GPa. Similarly, the range of C_{12} was 14.6 GPa and C_{44} was 15.4 GPa. With the increase of Cr content, the value of C_{11} increased from 208.1 GPa to 260.7 GPa, and the variation range of C_{12} and C_{44}

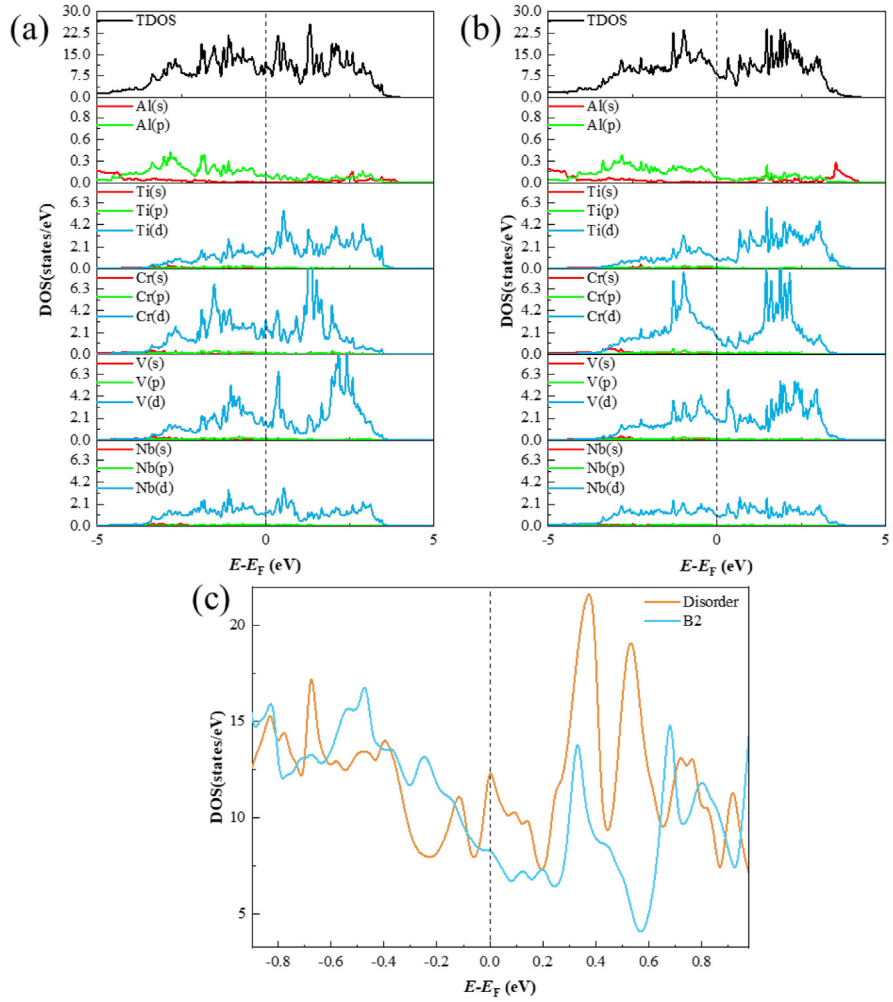

Fig. 3 – (a) TDOS and PDOS of disordered configuration AlTiCrVNb, (b) TDOS and PDOS of B2 configuration (V–Al–Cr) (V–Ti–Nb), vertical dashed line represents Fermi level (E_F), (c) TDOS near the Fermi level.

was 3.6 GPa and 10.5 GPa. The elastic constant C_{11} is the most sensitive to the variation of Ti and Cr contents.

With the increase of Ti content, both bulk modulus B and shear modulus G gradually decrease, while the B and G determined by Cr expressed inverse result. The Poisson's ratio and Pugh's ratio (B/G) of a material can be analyzed to determine whether the material is plastic or not, when the value of B/G is greater than 1.75, the material shows plasticity; on the

Table 1 – Mechanical properties of AlTiCrVNb in disordered and B2 ordered configurations.

Configuration	C_{11}	C_{12}	C_{44}	B	G	E	υ	B/G
Disorder	194.45	131.24	61.53	153.92	47.09	128.2	0.36	3.72
B2	227.46	123.11	59.98	154.92	56.73	151.67	0.33	2.73

Table 2 – Elemental content of each site in $Ti_xCrVNbAl$ and $Cr_xTiVNbAl$.

	(Al	Cr	V) $_\alpha$	(Ti	Nb	V) $_\beta$
$Ti_{0.5}CrVNbAl$	44.44%	44.44%	11.11%	22.22%	44.44%	33.33%
$Ti_{1.5}CrVNbAl$	36.36%	36.36%	27.27%	54.54%	36.36%	9.09%
$Ti_2CrVNbAl$	33.33%	33.33%	33.33%	66.66%	33.33%	0
$Cr_{0.5}TiVNbAl$	44.44%	22.22%	33.33%	44.44%	44.44%	11.11%
$Cr_{1.5}TiVNbAl$	36.36%	54.54%	9.09%	36.36%	36.36%	27.27%
$Cr_2TiVNbAl$	33.33%	66.66%	0	33.33%	33.33%	33.33%

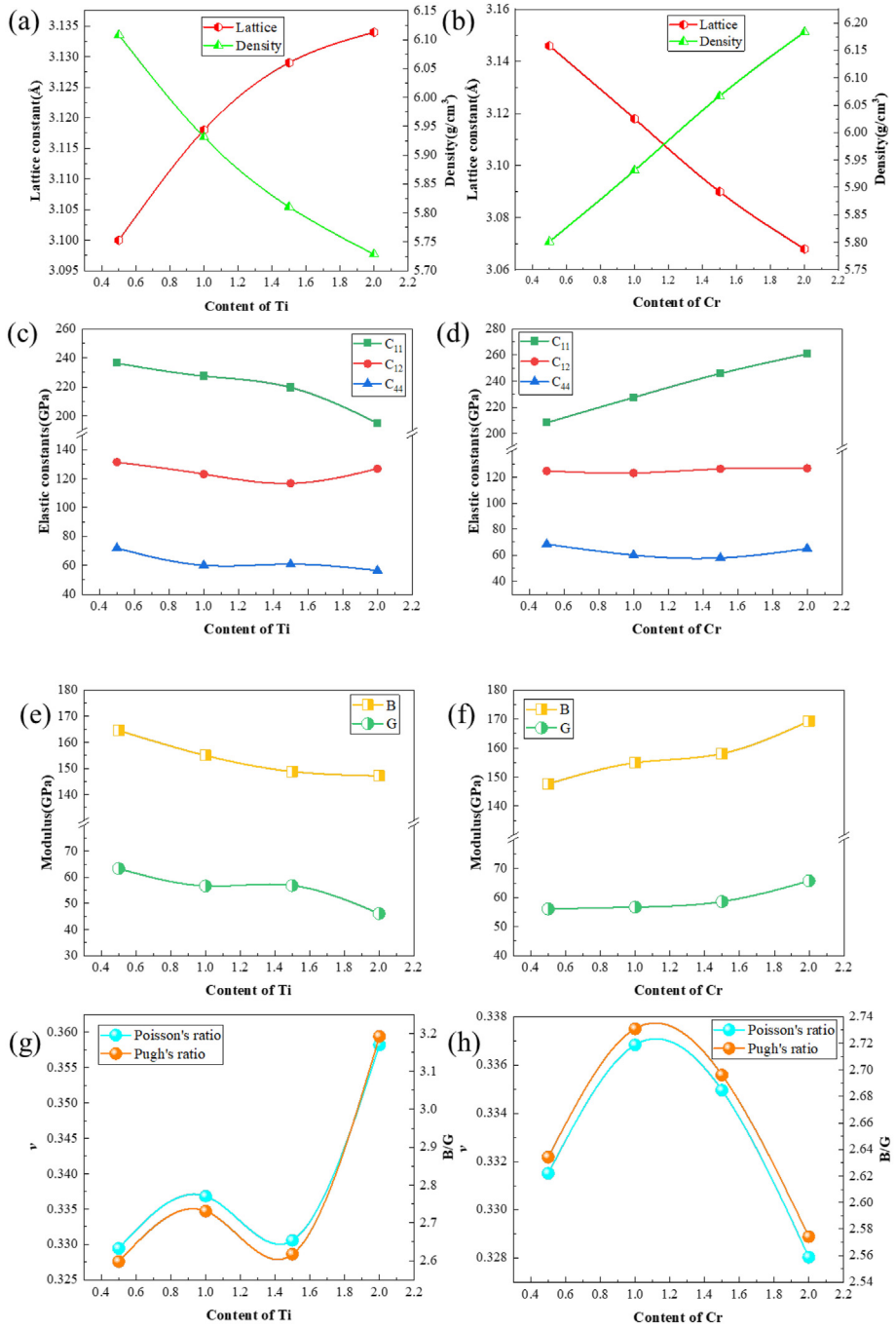

Fig. 4 – (a) (b) The lattice constants and densities corresponding to different Ti and Cr contents. (c) (d) Elastic constants corresponding to different Ti and Cr contents. (e) (f) Bulk modulus and shear modulus corresponding to different Ti and Cr contents. (g) (h) Poisson's ratio and Pugh's ratio corresponding to different Ti and Cr contents.

contrary, the material shows brittleness. The larger the ratio, the better the plasticity [38]. With the increase of Ti content, Poisson's ratio and Pugh's ratio increased first and then decreased, but they continuously increased finally. With the increase of Cr content, Poisson's ratio and Pugh's ratio increased first and then decreased. The influence of Ti content on the plasticity of the alloy is more complex, and there are obviously abnormal changes in the range of $x = 1$ to $x = 1.5$. From the general trend, the increase of Ti will increase the plasticity of the alloy, while the increase of Cr will decrease the plasticity of the alloy.

In order to verify the accuracy of the calculated results, the Young's modulus values of Ti_x and Cr_x($x = 0.5,1.5,2$) alloys were tested by nano-indentation experiment. Fig. 5 shows the values of Young's modulus obtained from nanoindentation experiments. It is clear that the calculated results are in good

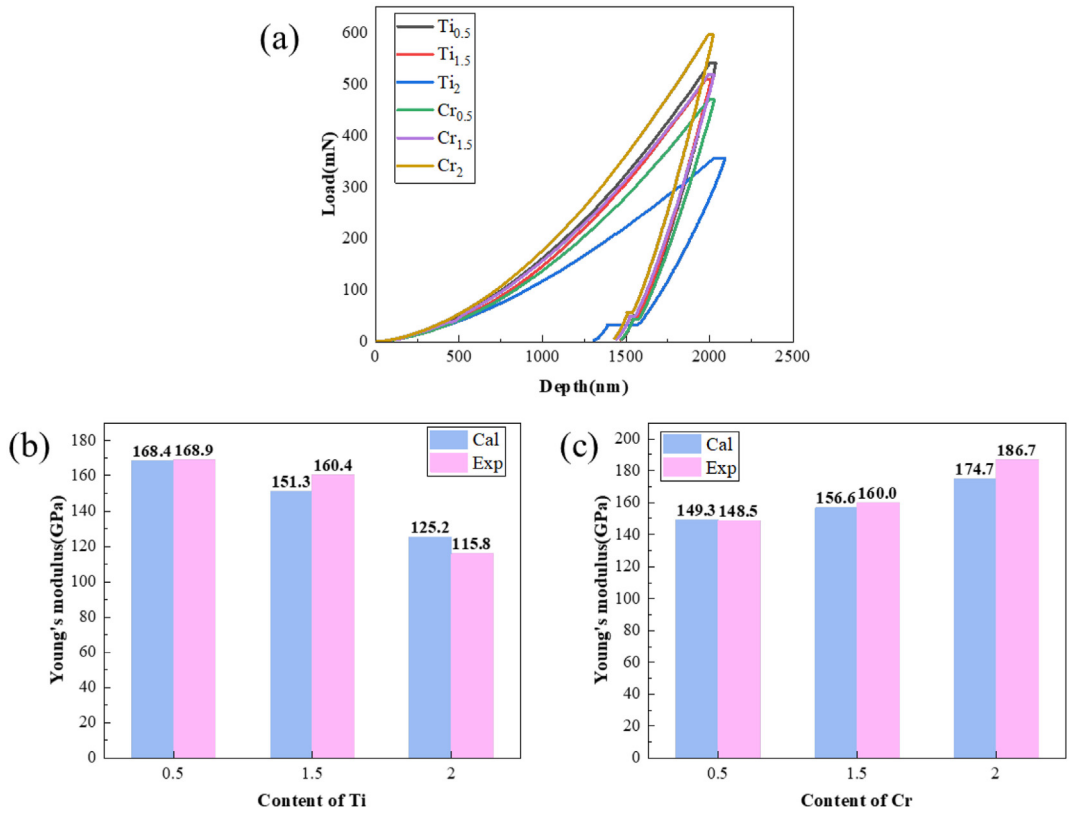

Fig. 5 – (a) Nanoindentation data (b) (c) Calculation and experimental values of Young's modulus of $Ti_xCrVNbAl$ and $Cr_xTiVNbAl$ high entropy alloys.

agreement with the experimental results. With the increase of Ti content, the Young's modulus of the alloy decreases. On the contrary, the increase of Cr content will increase Young's modulus. In summary, the increasement of Ti content provides more plasticity and lowers the strength while the increasement of Cr content provides more strength and lowers the plasticity. According to the results of ordered B2 and disordered BCC structures with equal molar ratio, a great influence was generated on the alloy's mechanical properties by B2 ordered structure and the B2 configuration's calculation results is similar to the experiment. It shows that the mechanical properties of the alloy are mainly affected by the ordered B2 phase, and the ordered B2 phase greatly improves the strength of the alloy.

4. Conclusion

In this study, the first principle method was used to describe the element occupation of equal molar ratio AlTiVCrNb HEAs and applied to non-equal atomic ration condition. The results show that Cr tends to occupy the sublattice of Al, Nb tends to occupy the sublattice of Ti, and V is randomly distributed between the two sublattices. The effect of chemical short-range order on lattice constants is very small, while there is obvious energy difference. Compared with the disordered BCC structure, the B2 ordered structure obviously improves the strength of the alloy, while greatly reducing the plasticity. The effects of Ti and Cr content on the mechanical properties of the alloy were analyzed based on the B2 ordered structure. High Ti content decreased the strength of the alloy, but it effectively improved the plasticity of the alloy. The increase of Cr content decreased the plasticity of the alloy, but it increased the strength of the alloy. The accuracy of the first principle calculation results is proved by experiments, which indicates that the mechanical properties of AlTiVCrNb HEAs could be reasonably predicted by the partial order modeling method and it's beneficial to composition design. The alloy with ideal properties can be obtained by adjusting the relative content of elements.

Declaration of Competing Interest

The authors declare that they have no known competing financial interests or personal relationships that could have appeared to influence the work reported in this paper.

Acknowledgements

This work was supported by the National Natural Science Foundation of China (52161028), Major Discipline Academic and Technical Leaders Training Program of Jiangxi Province (20213BCJ22017).

REFERENCES

[1] Yeh JW, Chen SK, Lin SJ, Gan JY, Chin TS, Shun TT, et al. Nanostructured high-entropy alloys with multiple principal elements: novel alloy design concepts and outcomes. Adv Eng Mater 2004;6(5):299–303. https://doi.org/10.1002/adem.200300567.

[2] Cantor B, Chang I, Knight P, Vincent A. Microstructural development in equiatomic multicomponent alloys. Mater Sci Eng, A 2004;375:213–8. https://doi.org/10.1016/j.msea.2003.10.257.

[3] Senkov O, Wilks G, Miracle D, Chuang C, Liaw P. Refractory high-entropy alloys. Intermetallics 2010;18(9):1758–65. https://doi.org/10.1016/j.intermet.2010.05.014.

[4] Senkov ON, Wilks G, Scott J, Miracle DB. Mechanical properties of Nb25Mo25Ta25W25 and V20Nb20Mo20Ta20W20 refractory high entropy alloys. Intermetallics 2011;19(5):698–706. https://doi.org/10.1016/j.intermet.2011.01.004.

[5] Senkov ON, Miracle DB, Chaput KJ, Couzinie J-P. Development and exploration of refractory high entropy alloys—a review. J Mater Res 2018;33(19):3092–128. https://doi.org/10.1557/jmr.2018.153.

[6] Nie X, Cai M, Cai S. Microstructure and mechanical properties of a novel refractory high entropy alloy HfMoScTaZr. Int J Refract Met Hard Mater 2021;98:105568. https://doi.org/10.1016/j.ijrmhm.2021.105568.

[7] Huang S, Li W, Eriksson O, Vitos L. Chemical ordering controlled thermo-elasticity of AlTiVCr1-xNbx high-entropy alloys. Acta Mater 2020;199:53–62. https://doi.org/10.1016/j.actamat.2020.08.005.

[8] Stepanov N, Shaysultanov D, Salishchev G, Tikhonovsky M. Structure and mechanical properties of a light-weight AlNbTiV high entropy alloy. Mater Lett 2015;142:153–5. https://doi.org/10.1016/j.matlet.2014.11.162.

[9] Yurchenko NY, Stepanov N, Zherebtsov S, Tikhonovsky M, Salishchev G. Structure and mechanical properties of B2 ordered refractory AlNbTiVZrx (x= 0–1.5) high-entropy alloys. Mater Sci Eng, A 2017;704:82–90. https://doi.org/10.1016/j.msea.2017.08.019.

[10] Qiu Y, Hu Y, Taylor A, Styles M, Marceau R, Ceguerra A, et al. A lightweight single-phase AlTiVCr compositionally complex alloy. Acta Mater 2017;123:115–24. https://doi.org/10.1016/j.actamat.2016.10.037.

[11] Soni V, Gwalani B, Alam T, Dasari S, Zheng Y, Senkov ON, et al. Phase inversion in a two-phase, BCC+B2, refractory high entropy alloy. Acta Mater 2020;185:89–97. https://doi.org/10.1016/j.actamat.2019.12.004.

[12] Senkov O, Jensen J, Pilchak A, Miracle D, Fraser H. Compositional variation effects on the microstructure and properties of a refractory high-entropy superalloy AlMo0. 5NbTa0. 5TiZr. Mater Des 2018;139:498–511. https://doi.org/10.1016/j.matdes.2017.11.033.

[13] Wang W, Zhang Z, Niu J, Wu H, Zhai S, Wang Y. Effect of Al addition on structural evolution and mechanical properties of the AlxHfNbTiZr high-entropy alloys. Mater Today Commun 2018;16:242–9. https://doi.org/10.1016/j.mtcomm.2018.06.004.

[14] Laube S, Chen H, Kauffmann A, Schellert S, Müller F, Gorr B, et al. Controlling crystallographic ordering in Mo–Cr–Ti–Al high entropy alloys to enhance ductility. J Alloys Compd 2020;823:153805. https://doi.org/10.1016/j.jallcom.2020.153805.

[15] Qiao D, Liang H, Wu S, He J, Cao Z, Lu Y, et al. The mechanical and oxidation properties of novel B2-ordered Ti2ZrHf0. 5VNb0. 5Alx refractory high-entropy alloys. Mater Char 2021;178:111287. https://doi.org/10.1016/j.matchar.2021.111287.

[16] Huang S. The chemical ordering and elasticity in FeCoNiAl1–xTix high-entropy alloys. Scripta Mater 2019;168:5–9. https://doi.org/10.1016/j.scriptamat.2019.04.008.

[17] Qiu S, Chen S-M, Naihua N, Zhou J, Hu Q-M, Sun Z. Structural stability and mechanical properties of B2 ordered refractory AlNbTiVZr high entropy alloys. J Alloys Compd 2021;886:161289. https://doi.org/10.1016/j.jallcom.2021.161289.

[18] Soven P. Coherent-potential model of substitutional disordered alloys. Phys Rev 1967;156(3):809. https://doi.org/10.1103/PhysRev.156.809.

[19] Gyorffy BL. Coherent-potential approximation for a nonoverlapping-muffin-tin-potential model of random substitutional alloys. Phys Rev B 1972;5(6):2382. https://doi.org/10.1103/PhysRevB.5.2382.

[20] Van de Walle A, Tiwary P, De Jong M, Olmsted D, Asta M, Dick A, et al. Efficient stochastic generation of special quasirandom structures. Calphad 2013;42:13–8. https://doi.org/10.1016/j.calphad.2013.06.006.

[21] Zunger A, Wei S-H, Ferreira L, Bernard JE. Special quasirandom structures. Phys Rev Lett 1990;65(3):353. https://doi.org/10.1103/PhysRevLett.65.353.

[22] Kresse G, Furthmüller J. Efficient iterative schemes for ab initio total-energy calculations using a plane-wave basis set. Phys Rev B 1996;54(16):11169. https://doi.org/10.1103/PhysRevB.54.11169.

[23] Kresse G, Furthmüller J. Efficiency of ab-initio total energy calculations for metals and semiconductors using a plane-wave basis set. Comput Mater Sci 1996;6(1):15–50. https://doi.org/10.1016/0927-0256(96)00008-0.

[24] Ernzerhof M, Scuseria GE. Assessment of the perdew–burke–ernzerhof exchange-correlation functional. J Chem Phys 1999;110(11):5029–36. https://doi.org/10.1063/1.478401.

[25] Hammer B, Hansen LB, Nørskov JK. Improved adsorption energetics within density-functional theory using revised Perdew-Burke-Ernzerhof functionals. Phys Rev B 1999;59(11):7413. https://doi.org/10.1103/PhysRevB.59.7413.

[26] Perdew JP, Burke K, Ernzerhof M. Generalized gradient approximation made simple. Phys Rev Lett 1996;77(18):3865. https://doi.org/10.1103/PhysRevLett.77.3865.

[27] Blöchl PE. Projector augmented-wave method. Phys Rev B 1994;50(24):17953. https://doi.org/10.1103/PhysRevB.50.17953.

[28] Kresse G, Joubert D. From ultrasoft pseudopotentials to the projector augmented-wave method. Phys Rev B 1999;59(3):1758. https://doi.org/10.1103/PhysRevB.59.1758.

[29] Monkhorst HJ, Pack JD. Special points for Brillouin-zone integrations. Phys Rev B 1976;13(12):5188. https://doi.org/10.1103/PhysRevB.13.5188.

[30] Murnaghan FD. The compressibility of media under extreme pressures. Proc Natl Acad Sci U S A 1944;30(9):244–7. https://doi.org/10.1073/pnas.30.9.244.

[31] Birch F. Finite elastic strain of cubic crystals. Phys Rev 1947;71(11):809. https://doi.org/10.1103/PhysRev.71.809.

[32] Le Page Y, Saxe P. Symmetry-general least-squares extraction of elastic data for strained materials from ab initio calculations of stress. Phys Rev B 2002;65(10):104104. https://doi.org/10.1103/PhysRevB.65.104104.

[33] Zuo L, Humbert M, Esling C. Elastic properties of polycrystals in the Voigt-Reuss-Hill approximation. J Appl Crystallogr 1992;25(6):751–5. https://doi.org/10.1107/S0021889892004874.

[34] Skriver HL. Crystal structure from one-electron theory. Phys Rev B 1985;31(4):1909. https://doi.org/10.1103/PhysRevB.31.1909.

[35] Söderlind P, Eriksson O, Wills J, Boring A. Theory of elastic constants of cubic transition metals and alloys. Phys Rev B 1993;48(9):5844. https://doi.org/10.1103/PhysRevB.48.5844.
[36] Calin M, Helth A, Moreno JJG, Bönisch M, Brackmann V, Giebeler L, et al. Elastic softening of β-type Ti–Nb alloys by indium (In) additions. J Mech Behav Biomed Mater 2014;39:162–74. https://doi.org/10.1016/j.jmbbm.2014.07.010.
[37] Born M. On the stability of crystal lattices. I. Math Proc Cambridge Philos Soc 1940;36(2):160–72. https://doi.org/10.1017/S0305004100017138.
[38] Pugh S. XCII. Relations between the elastic moduli and the plastic properties of polycrystalline pure metals. Philos Mag A 1954;45(367):823–43. https://doi.org/10.1080/14786440808520496.